Material Properties for Welding Simulation — Measurement, Analysis, and Exemplary Data

It has been found that in the given application case from the automotive industry with laser beam welding flat plates, the most important boundary conditions for measurement are high heating and cooling rates

BY C. SCHWENK AND M. RETHMEIER

ABSTRACT

Welding is a key technology in the area of industrial production due to its flexibility and efficiency. However, new materials and welding techniques necessitate permanent research activities in order to keep up with the demands. A detailed knowledge about the process itself and the heat effects of welding, e.g., temperatures, distortions, and stresses, is the basis for a target-oriented optimization instead of a trial-and-error approach. Numerical welding simulation is a powerful tool to meet these demands. Complementary to an experimental investigation, it enables the analysis of the specimen during the welding process, commonly known as computational welding mechanics (CWM). Whereas simulation is nowadays a common tool in different development processes, the modeling of welding still remains difficult because of the multiple physical effects taking place. One of the most important problems for the user is the lack of knowledge about the material properties as input data for the simulation. Furthermore, any scattering of the data causes uncertainties that can have major effects on the calculations. The objective of this paper is to give an overview about the experimental determination and analysis of the material properties needed as input data for a welding simulation. The measurement techniques and the occurring deviations of the results are discussed. Additionally, the collected data for three representative alloys (dual-phase steel, austenitic steel, precipitation-hardenable aluminum alloy) are analyzed. Finally, the temperature-dependent thermophysical and thermomechanical material properties for these three alloys are given in a ready-to-use format for a numerical welding simulation.

Introduction and Motivation

The flexibility and efficiency of modern welding techniques are main factors for their wide range of application in the industrial production process. Due to continuous development of materials, e.g., high-strength, fine-grain steels, as well as new welding techniques, e.g., laser-arc hybrid welding, ongoing research work is necessary to guarantee the quality of joined components.

Today, numerical simulation by means of a finite element analysis is a common tool in the development process of a large number of industrial products and helps to investigate the new material and welding technique combinations as stated above. Nevertheless, the numerical analysis of the welding process and its effects on the specimen still remain difficult because of the multiple physical effects involved (Refs. 1, 2). The numerical welding simulation enables the detailed analysis of the heat effects of welding, i.e., the thermal and mechanical behavior of the specimen during welding. The understanding of these influences is the basis for an optimization of welded parts with respect to quality aspects like distortions and stresses (Ref. 3). Additionally, the influence of single parameters can be investigated without any coupling effects that normally occur during real welding experiments.

One of the most important challenges in welding simulation is the lack of temperature- and phase-dependent material properties that are needed as input data. For most modern alloys, these data are not available, neither from the supplier nor in the literature. Consequently, an experimental determination of the values is often required in order to get high-quality simulation results. One remaining problem is the inevitable scattering of the experimental data, especially at relatively high temperatures. These uncertainties can have major effects on the subsequently calculated temperatures, distortions, and stresses (Refs. 4, 11).

In the following sections, the aspect of the experimental material property determination is investigated considering the special conditions during welding and its numerical simulation. This is done with respect to the special needs in the automotive industry because it resembles a key user for computational welding mechanics (CWM). Here, welding of thin metal sheets in car body production is a central task. One of the most important aspects is the high heating and cooling rates during the process. The investigated alloys — the high-strength, dual-phase steel DP-W 600 (1.0936), the austenitic steel H400 (1.4376), and the precipitation-hardenable aluminum alloy Ecodal 608 (EN AW-6181) — are common representatives in the automotive industry.

KEYWORDS

Thermophysical Material Properties
Thermomechanical Material Properties
Experimental Determination
Numerical Welding Simulation

Considered Alloys

The alloys considered in this paper are not only typical for automotive applications, but they are additionally chosen for a detailed sensitivity analysis of the material properties with respect to calculated welding temperature fields and distortions (Ref. 4). In this section, the criteria for the

C. SCHWENK (christopher.schwenk@bam.de) *and M. RETHMEIER are with the Federal Institute for Materials Research and Testing (BAM), Division 5.5, "Safety of Joined Components," Berlin, Germany.*

selection of the actual alloys, their alloying contents, and their typical characteristics are discussed. The decision for the specific alloy was driven by two reasons. First, for a simulation and a sensitivity analysis, a comparison of different alloys and alloy groups is interesting. Second, all alloys in these groups should be in use in the automotive industry.

For the selected alloy groups (ferritic steel with phase transformation, austenitic steel without phase transformation, aluminum alloy), there are different possible ways of comparison. First of all, both steel alloys can be compared whereas the different metallurgical behaviors of the ferritic and austenitic steel, here for example the phase transformation, is of interest. Additionally, the two alloys cover, in a general view, both groups of low-alloyed and high-alloyed steels. Because of the small differences of the thermophysical properties, in contrast to the thermomechanical ones of specific alloys within their respective groups, they can also serve as rough data for future temperature field simulations of similar or future alloys with comparable alloying content. Furthermore, the comparison of the two materials not undergoing phase transformations, namely the austenitic steel and aluminum alloy, with the ferritic steel with phase transformation is interesting. Finally, the differences between the steels and aluminum alloy are of interest.

The investigated material for the group of low-alloyed steel with phase transformation is DP-W 600, a typical representative for high-strength steels in the automotive industry. For the high-alloyed austenitic steel, the decision fell upon Nirosta H400. This alloy was designed especially for automotive applications and can be used as a cost-effective alternative to the common steel 1.4301 (X5CrNi18 10). While keeping the mechanical properties at a comparable level, the production price is lower because of a reduced nickel content. A higher content of nitrogen as a partial surrogate for the nickel ensures a high work-hardening behavior. The selection of Ecodal 608 was driven by the fact that it is a standard material used for nonvisual inner parts where the critera of lightweight characteristics and strength are important. In the following sections each of the three materials, their alloy contents, and the corresponding typical mechanical properties are given.

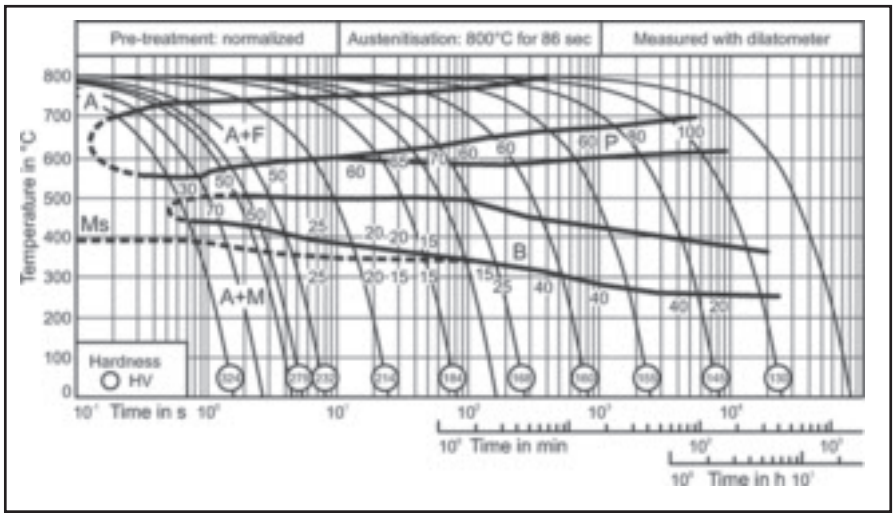

Fig. 1 — Continuous cooling transformation diagram of DP-W 600 (1.0936) according to supplier data sheet (Ref. 12).

High-Strength, Dual-Phase Steel DP-W 600 (1.0936)

The steel DP-W 600 with the material number 1.0936 is a hot-rolled, thermomechanically treated dual-phase steel. It has a high strength, good cold forming capabilities, and due to its low carbon content, excellent weldability qualities. This steel has certain advantages for the lightweight construction of cold formed parts in the automotive industry, e.g., undercarriage parts, body-in-white reinforcements, and profiles. Its high strain-hardening capabilities lead to a strong increase in the yield strength even for small degrees of deformation.

The chemical composition and carbon equivalents PCM and CET based on the

Table 1 — Chemical Composition of DP-W 600 According to Supplier Data Sheet (first row, [Ref. 12]) and Own Measurements (second row and below)

C	Si	Mn	P	S	$Al_{ges.}$	Cr + Mo	B
≤0.12	≤1.50	≤0.15	≤0.060	≤0.010	≥0.015	≤1.0	≤0.005
C	Si	Mn	P	S	Al	Cr	Mo
0.0086	0.104	1.573	0.017	0.001	1.16	0.452	0.009
B	Ni	Ti	Nb	Zr	V	W	Co
0.003	0.02	0.009	0.005	0.005	0.006	0.042	0.008
Cu	Ca	N	Pb	Sn	As	Sb	Te
0.019	0.0012	0.006	0.01	0.004	0.004	0.01	0.002
Zn	Mg						
0.014	0.003						

Carbon equivalent PCM: 0.117 mass-%

Carbon equivalent CET: 0.191 mass-%

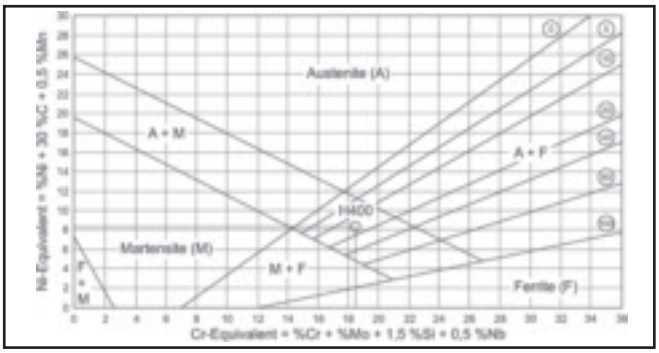

Fig. 2 — Schaeffler diagram for Cr-Ni steels according to Schuster (Ref. 14).

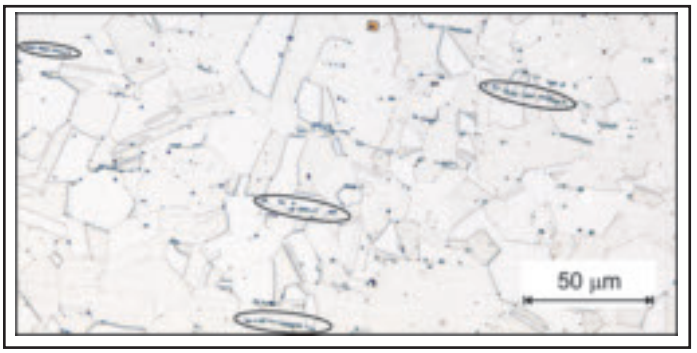

Fig. 3 — Microsection of base material H400 (marked: banded delta ferrite).

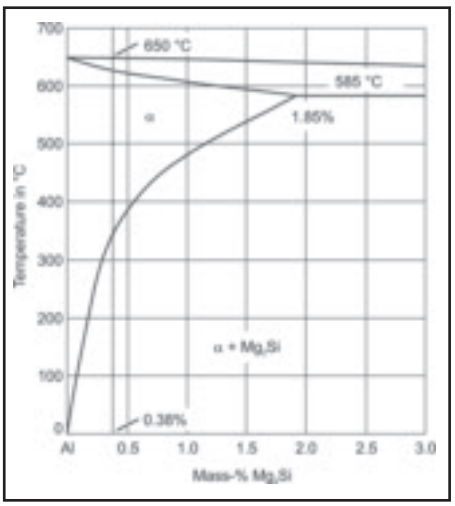

Fig. 4 — Phase diagram of the system Al-Mg_2Si (Ref. 16).

measured values are given in Table 1. The typical mechanical properties according to the manufacturer's datasheet are stated in Table 2. The continuous cooling transformation (CCT) diagram of the alloy provided by the manufacturer is shown in Fig. 1.

Austenitic Steel H400 (1.4376)

The steel Nirosta H400 with the material number 1.4376 is a high-strength, corrosion-resistant stainless steel. It can be welded with nearly all established welding techniques and has, due to its metastable austenitic microstructure, a good ratio between strength and formability. However, during manufacturing processes, including cold forming, it needs higher forces and has a more significant springback behavior compared to standard Cr-Ni steels. The typical mechanical properties are listed in Table 3.

The chemical composition according to the manufacturer's data and to our own spark emission spectroscopy measurements are stated in Table 4. The actual nickel content is 3.8% and is slightly above the allowed maximum value. This leads, according to the Schaeffler diagram in Fig. 2, to a smaller amount of the unwanted delta ferrite and hence has positive effects for the weldability.

The position for H400 is indicated in the diagram with the chrome and nickel equivalent according to Schuster (Ref. 14). The position of the alloy is not fully in the austenitic area but in the austenitic-ferritic mixed zone. Figure 3 shows a microsection of the base material where, beside the austenite, some carbides and small amounts of delta ferrite are visible.

Due to its positive characteristics like corrosion resistance, ultimate tensile strength, and, because of the work-hardening behavior, high-energy dissipation during crash, it is predestined for automotive applications. Typical parts are space frame structure parts or undercarriage assemblies.

Table 2 — Mechanical Properties of DP-W 600, As-Delivered Condition at Room Temperature Values According to Supplier Data Sheet (Ref. 12)

$R_{p0.2}$ in MPa	R_m in MPa	A_5 in %	A_{80} in %
330–450	580	24	20

Table 3 — Mechanical Properties of H400 (1.4376), As-Delivered Condition at Room Temperature Values According to Supplier Data Sheet (Ref. 13)

$R_{p0.2}$ in MPa	$R_{p1.0}$ in MPa	R_m in MPa	A_5 in %
400	420	600–900	≥41

Aluminum Alloy Ecodal 608 (EN AW-6181)

The Aluminum Alloy Ecodal 608 with material number EN AW-6181 (Ref. 17) is a copper-free AlMgSi alloy with very good cold forming behavior and strain hardening effects. It can be age hardened at room temperature and has a low-corrosion aptitude. Furthermore, it was specially designed for the recycling of different aluminum alloys to reduce energy and material consumption during manufacturing. The typical mechanical properties are given in Table 5 whereas Table 6 shows the chemical composition based on measured values. The calculated content, based on the measured values, of Mg_2Si particles is approximately 0.38%. This value is included in the quasi binary Al-Mg_2Si phase diagram in Fig. 4.

The applications of Ecodal 608 are mainly inner sections and reinforcements in automotive applications like sections of the front lid, hatchback, or doors. These parts normally have lower requirements for the surface quality than outer parts with direct visibility. Hence, a lightweight and cost-effective construction can be reached at the same time.

The main material properties of an alloy to be used for a numerical welding simulation cover the thermophysical and thermomechanical behavior of the material. The following section gives a detailed overview about what general aspect of the material data is required in order to perform a welding simulation.

Required Material Properties and Temperature Range

As already stated, the numerical welding simulation requires a wide range of material properties as input data. Considering the temperature field calculation, the thermophysical properties

- density ρ
- specific heat capacity c_P
- thermal conductivity λ

are needed. Instead of the specific heat capacity and the density, the user can also use the enthalpy of the alloy. For the calculation of the distortions and stresses, the thermomechanical properties

- yield strength $R_{p0,2}$
- hardening behavior
- Young's modulus E
- thermal expansion ε_{th}
- Poisson's ratio ν

are a prerequisite. All these properties have to be temperature dependent from room temperature up to solidus temperature and above. The calculated temperatures can easily reach values of 2500°C and more, and the numerical approach presupposes available data for all the temperatures that occur. From the experimental point of view, the measurement at these temperatures is, in most cases, extremely difficult or even impossible, especially for the thermomechanical properties. A common practical compromise is the measurement of the properties from room temperature up to approximately 0.8 $T_{Solidus}$ of the alloy. In addition to this wide temperature range, alloys with phase transformation are needed phase dependent (e.g., ferrite, austenite, bainite, martensite) including the CCT diagram.

The correct measurement of the needed properties is a demanding task with respect to time, costs, and accuracy, especially with rising temperatures and for alloys with phase transformation like the DP-W 600. Some measurement techniques that are suitable for this task as well as the corresponding equipment are described in the following section. Further information about specific measurement devices that could be suitable can be found, for example, in Ref. 6.

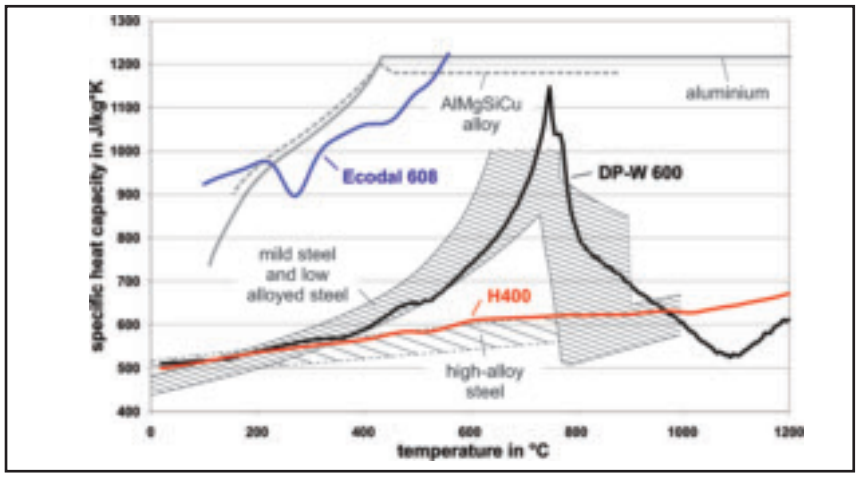

Fig. 5 — Comparison of experimentally determined specific heat capacity c_p and literature values; reference data adopted from Radaj (Ref. 1) and Richter (Refs. 7, 8).

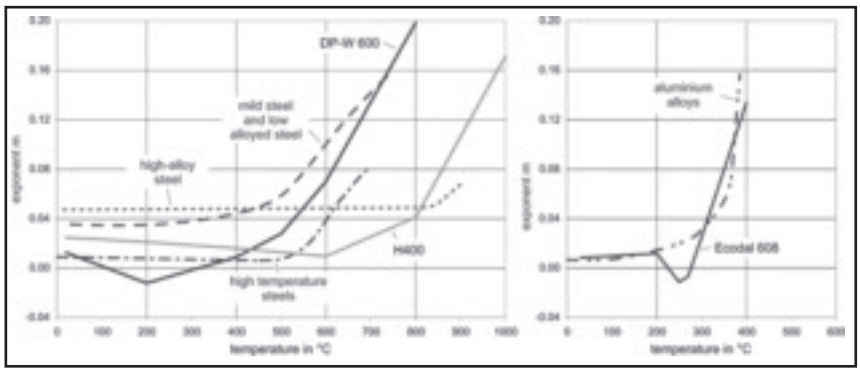

Fig. 6 — Comparison of exponent m for measured data and literature values. Left graph: steels; right graph: aluminum alloys. Adopted from Makhnenko (Ref. 9).

Measurement Techniques with Respect to Welding Conditions

The measurement of the required material properties covers a thermophysical and thermomechanical part. During all experiments, one has to take care that the rising temperatures do not affect the surface of the material. In order to prevent scaling that can influence the accuracy of

Table 4 — Chemical Composition of H400 According to Supplier Data Sheet (first row, Ref. 13) and Own Measurements (second row and below)

C	Si	Mn	P	S	Cr	Ni	N
≤0.12	≤1.50	≤0.15	≤0.060	≤0.010	≥0.015	≤1.0	≤0.005
C	Si	Mn	P	S	Cr	Ni	N
0.03	0.469	7.129	0.027	0.003	17.5	3.795	0.25
Mo	Al	Ti	Nb	Zr	V	W	Co
0.298	0.001	0.012	0.013	0.013	0.06	0.015	0.093
B	Ca	Cu	Pb	Sn	As	Sb	Te
0.0	0.0007	0.195	0.011	0.006	0.007	0.001	0.004
Zn	Mg						
0.012	0.003						

Carbon equivalent PCM:1.376 mass-%

Carbon equivalent CET: 1.752 mass-%

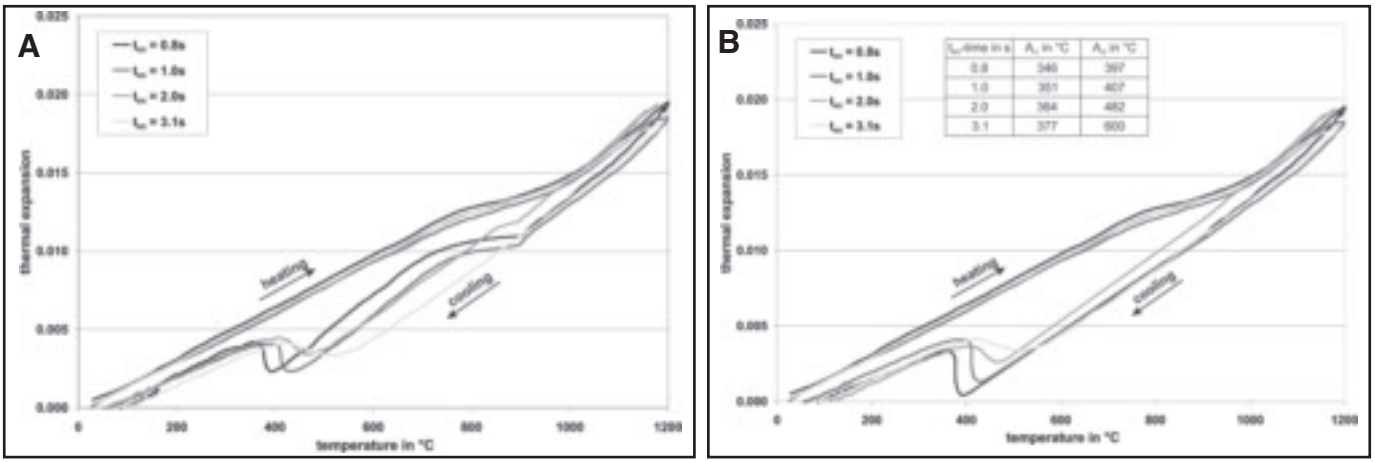

Fig. 7 — Measured thermal expansion for DP-W 600 for different $t_{8/5}$ times. A — Raw data; B — corrected curves for high cooling rates; transformation temperatures derived in accordance with Ref. 10.

optical detection methods, all measurements should be done under an inert atmosphere.

For the thermophysical data, one special aspect has to be taken into account. The material used in the automotive industry is often, like the DP-W 600, coated with zinc to prevent corrosion. These coatings have to be removed prior to the measurements because a clean and matt surface is needed for the correct measurement of the thermal diffusivity $a(T)$ using a laser flash method. The density $\rho(T)$ and the specific heat capacity $c_p(T)$ can be determined using commercially available equipment and standard specimen preparation. After the experiments, a calculation of the thermal conductivity $\lambda(T)$ as input for the simulation is done using the gathered data in combination with Equation 1.

$$\lambda(T) = a(T) \cdot \rho(T) \cdot c_p(T) \qquad (1)$$

The measurement of the thermomechanical material properties has to be done with consideration of two important aspects that are characteristically for welding. Depending on the welding technique and specimen thickness, the heating and cooling rates can be very high. While the heating rate has a direct influence on the strain rates and therefore, the yield strength and hardening behavior of the material, the cooling rate is an important factor for the phase transformation effects of an alloy and the corresponding thermal expansion.

The tensile tests for the determination of the yield strength and hardening behavior have to be executed with both a quasistatic and at least one higher strain rate $\dot{\varepsilon}$. The latter can be approximated very roughly using the thermal expansion coefficient at room temperature α_{RT} as stated in the simplified Equation 2

$$\dot{\varepsilon} = \alpha_{RT} \cdot \dot{T} = \alpha_{RT} \cdot \frac{\Delta T}{\Delta t} \qquad (2)$$

For example, the temperature rate for laser beam welding with high power and velocity can easily reach $\dot{T} = 4000\ K/s$. With an assumed averaged thermal expansion coefficient of $\alpha_{st} = 1.3 \cdot 10^{-5}/K$ for steel and $\alpha_{al} = 2.5 \cdot 10^{-5}/K$ for aluminum alloys, the strain rates during laser beam welding can be estimated to values of $\dot{\varepsilon}_{st} = 0.05/s$ and $\dot{\varepsilon}_{al} = 0.1/s$ in correspondence with literature values (Ref. 5). These values have to be adapted to the welding technique that has to be simulated. For other processes like gas metal arc welding (GMAW) or gas tungsten arc welding (GTAW), different heating rates are typical.

In the measurement setup of a tensile test at elevated temperatures, the testing machine should be run in distance control mode rather than force control mode for the following reason. At certain conditions with a special combination of temperature and strain rate, metallurgical effects can cause problems using the machine while running in force control mode. In such cases, the measured curves can show a step-like behavior because of the Portevin-LeChatelier effect where the atomic diffusion in the material has the same velocity as the movement of the dislocations. The movement of the dislocations is time and again locked, resulting in a fluctuation of the material flow and stiff-

Table 5 — Mechanical Properties of Ecodal 608 (EN AW-6181), As-Delivered Condition at Room Temperature, Values According to Supplier Data Sheet (Ref. 15)

$R_{p0.2}$ in MPa	R_m in MPa	A_{gl} in %	A_{80} in %
105	215	22	24

Table 6 — Chemical Composition of Ecodal 608 According to Supplier Data Sheet (first row, [Ref. 15]) and Own Measurements (second and third rows)

Si	Fe	Cu	Mn	Mg	Cr	Zn	Ti	others
0.7–1.1	≤0.5	≤0.25	≤0.4	0.6–1.0	≤0.15	≤0.3	≤0.25	≤0.15
Si	Fe	Cu	Mn	Mg	Cr	Zn	Ti	Al
0.812	0.244	0.045	0.017	0.757	0.012	0.02	0.028	98
Ni	Zr	V	Co	B	Ca	Pb	Sn	
0.003	0.001	0.007	0.001	0.001	0.0025	0.001	0.001	

ness of the specimen. This leads to problems in the force control of the testing machine, viewable in the tensile test plots, and can be overcome using the distance control mode. If needed in the simulation software, the hardening coefficient can be calculated subsequently using the measurement data (Ref. 18). Additionally, tensile tests of the fusion zone, e.g., by using microspecimen, can be very useful and are recommended because the values in the fusion and heat-affected zone (HAZ) can differ significantly from the base material values for some alloys.

The Young's modulus of the alloys should not be derived from tensile test results. Especially with rising temperatures and higher strain rates, the gradient at the beginning of the data curves normally shows very high scattering. Instead, this value can be measured much more accurately with an ultrasonic device. Here, the specific vibration answer of a geometrically defined specimen that is stimulated with an ultrasonic wave of known properties is measured, and the difference can be recalculated to the Young's modulus. Nevertheless, the extracted values should be cross checked with the tensile tests later on.

As stated above, the cooling rates have a direct influence on the phase transformation behavior and corresponding thermal expansion. This fact has to be accounted for the measurement of the thermal expansions, i.e., the dilatometric curves of the alloys. One typical information for the weldability of alloys is the cooling time between temperatures of 800° and 500°C, the so-called $t_{8/5}$ time. During high-power welding processes with a concentrated heat input such as laser beam welding, extremely low $t_{8/5}$ times of less than a second are possible and have to be reached also in the experiments. As for the tensile tests, the welding technique has a significant influence on the cooling rates, too, and leads to different $t_{8/5}$ times, e.g., for GMAW or GTAW processes.

The thermal expansion of a specimen undergoing high heating and cooling rates is normally measured with a special dilatometric device, e.g., a Gleeble machine. Here, $t_{8/5}$ times of about three seconds for a thin sheet metal specimen can be reached with passive cooling via the clamping devices. In contrast to that, the extremely low $t_{8/5}$ times during laser beam welding of less than a second necessitate an active cooling that can be done using a direct gas spray on the specimen with an inert gas. As is shown in the following section, this causes problems for the optical measurement of the lateral contraction of the specimen and leads to deviations in the monitored dilatometric curves. The thermal expansion experiments have to be executed with a variation of the $t_{8/5}$ time in order to monitor the phase transformation correctly and get the correct temperature intervals of the transformation. Caused by the very short heating and cooling of the specimen, the appearance of a small hysteresis between both cycles is normal and, in most cases, inevitable. The reference temperature that has been used for the experiments has to be given; for the material properties presented in Appendix A, it was 20°C.

The temperature-dependent measurement of the Poisson's ratio is not necessary when doing a distortion calculation because the influence on the results is negligible. Our own investigations show that the room-temperature value from the literature is sufficient for a welding simulation (Refs. 4, 6).

The correct measurement of the material properties is only the first step for the generation of a data set suitable for a numerical welding simulation. Equally important is the plausibility check of the raw data and the comparison with scatter bands of well-known alloys from literature or previous experiments as it is shown in the next section.

Plausibility Check and Analysis of Data

After the experimental determination of the material properties, these collected data have to be analyzed to ensure the correctness of the measurements and check its appropriateness for a numerical welding simulation. This is important because the material property data have a strong and direct influence not only on the result quality but also on the convergence behavior of the numerical calculation and, as a result, on the overall computation time.

The cross check of the measurement data with scatter bands from literature values is shown exemplarily in Fig. 5 for the specific heat capacity of the three alloys. Both the austenitic steel H400 and dual-phase steel DP-W 600 are well within the scatter bands for high-alloy steel and mild steel, respectively. The data show only minor scattering; the progression of the graphs is smooth. The curve for Ecodal 608 shows some characteristics that have to be investigated. The general behavior is consistent with the data for pure aluminum and AlMgSiCu taken from Richter (Refs. 7, 8). Nevertheless, the deviations in certain temperature intervals are significant.

The local minimum in the temperature range between 200° and 300°C is caused by an extensive precipitation of Mg_2Si particles and the subsequent dissolution. Our own analyses show that this local minimum of the specific heat capacity has only small effects on the calculated temperature field, and the following macroscopic mechanical behavior, and can be neglected (Ref. 6). As stated above, such local effects in the material data curves can have a major effect on the convergence and computation time. Other examples for a similar nonlinear behavior are the specific heat capacity peak of the phase transformation or latent heat of fusion. If the peaks have to be considered in the material data set because their influence cannot be neglected, one possible solution is to stretch extremely steep or stepwise peaks over a slightly larger temperature interval. The effects on the result quality are negligible, but the convergence behavior is, in most cases, improved a lot. Finally, the temperature range in which the peak of the specific heat capacity is implemented should be given together with the temperature-dependent values.

As stated at the description of the measurement techniques, the strain rate effect during tensile tests can be significant due to the high strain rates during welding. The combined effect of the temperature and strain rate on the yield strength can be checked in accordance with Equation 3 proposed by Makhnenko (Ref. 9).

$$\frac{\sigma_y(T)}{\sigma_{y,0}(T)} = \left(\frac{\dot{\varepsilon}}{\dot{\varepsilon}_0} \right)^{m(T)} \quad (3)$$

Here, the parameters are the yield strength $\sigma_y(T)$ at the temperature T and strain rate $\dot{\varepsilon}$ as well as the yield strength $\sigma_{y,0}(T)$ at the quasi static strain rate $\dot{\varepsilon}_0$. The temperature- and alloy-dependent exponent $m(T)$ is a measure for the dependence of the yield strength $\sigma_y(T)$ during a variation of the strain rates. A high value of the exponent $m(T)$ stands for a high dependency of the yield strength from the strain rate. In Fig. 6, one can see the extracted measurement data in comparison with literature values from Makhnenko (Ref. 9). In Fig. 6, on the left graph, it is visible that for the dual-phase steel DP-W 600, the strain rate influence becomes significant for temperatures above 500°C while the yield strength of the austenitic steel H400 is up to 700°C independent of the strain rate. Looking at the values for Ecodal 608, see the right graph of Fig. 6, one can see that the strain rate effect becomes visible for temperatures above 300°C. The information gathered using Equation 3 indicates that the tensile tests at elevated temperatures have to be executed with different strain rates for temperatures above 500°C for DP-W 600, 700°C for H400, and 300°C for Ecodal 608. Dependent on the desired simulation results (see Ref. 19 as well) and their quality, the user has to decide if it is needed to consider a strain rate dependent material behavior in the simulation model.

The experimental raw data for the

thermal expansion, i.e., the dilatometric curves, are shown exemplarily for DP-W 600 in Fig. 7A. The heating branch of the curves shows no noteworthy deviations for all four measurements. In contrast to that, in the cooling branch between 900° and 400°C, the curves for all cooling times except $t_{8/5}$ = 3.1 s are deviated. The responsible effect is the active cooling of the specimen with inert gas causing flickering effects. While needed to reach the high cooling rates, it interferes with the optical measurement of the specimen as described in the preceding section.

For the usage in the numerical simulation, the cooling branch of the curves achieved with active cooling have to be corrected using the general characteristic of the $t_{8/5}$ = 3.1 s curve with passive cooling — Fig. 7B. These corrected curves can now also be used to evaluate the required transformation temperatures Ar_1 and Ar_3 for the correct description of the CCT behavior. Using the standardized method in Ref. 10 leads to the derived values given in Fig. 7B.

The exemplary analysis of the measurement data gives an overview of the possible scattering of the material properties. A detailed plausibility check of the data is needed to derive a high-quality material property data set from the raw data of the measurements and is strongly recommended. The analysis methods help to identify possible systematic measurement errors. The temperature-dependent thermophysical and thermomechanical material properties for three different alloys are given as a result of the preceding measurements and plausibility checks. They can be found in the appendix and are represented in a ready-to-use format for a numerical welding simulation.

Summary and Conclusions

A numerical simulation of the welding-induced temperature field and corresponding distortions helps to investigate the heat effects of welding and, in the long run, to optimize the quality of welded parts. Due to the complexity of the welding process itself, the material property data for the simulation has to be temperature and phase dependent. The experimental determination of these data are, especially at the needed high-temperature values, very error prone. In the given exemplary application case from the automotive industry with laser beam welding of flat plates, the most important boundary conditions for the measurement are high heating and cooling rates.

The special characteristics of welding and its numerical calculation lead to the following aspects that have to be taken into account during the experiments. In general, all measurements have to be executed with an inert gas atmosphere to prevent scaling, and any coatings on the sheet metal have to be removed prior to the measurements.

The high heating rates cause high occurring strain rates that have an influence on the yield strength and hardening behavior of the material. Tensile tests at elevated temperatures have to be executed with a quasistatic and higher strain rate for certain temperatures dependent on the investigated alloy, here above 500°C for a dual-phase steel, above 700°C for an austenitic steel, and above 300°C for an aluminum alloy.

The high cooling rates, i.e., low $t_{8/5}$ times, in the order of less than one second necessitate an active cooling of the specimen with an inert gas during the dilatometric curve measurement. This can lead to measurement problems that have to be taken into account during the interpretation of the data, especially for alloys undergoing phase transformation, in order to guarantee a correct replication of the CCT behavior and transformation temperatures.

References

1. Radaj, D. 2003. *Welding Residual Stresses and Distortion: Calculation and Measurement*. English Edition, Volume 2, Düsseldorf, DVS-Verlag.

2. Radaj, D., Lundbäck, A., and Lindgren, L. E. 2007. Verification and validation in computational welding mechanics. *Mathematical Modelling of Weld Phenomena* (8). Eds. H. Cerjak, H. K. D. H. Bhadeshia, and E. Kozeschnik. Verlag der Technischen Universität Graz, pp. 1039–1051.

3. Babu, S. S., Sonnenberg, G., Schwenk, C., Goldak, J., Porzner, H., Khurana, S. P., Zhang W., and Gaylor, J. 2010. How can computational weld mechanics help industry? *Welding Journal* 89(11): 40–45.

4. Schwenk, C., Rethmeier, M., Dilger, K., and Michailov, V. 2007. Sensitivity analysis of welding simulation depending on material properties value variation. *Mathematical Modelling of Weld Phenomena* (8). Eds. H. Cerjak, H. K. D. H. Bhadeshia, and E. Kozeschnik. Verlag der Technischen Universität Graz, pp. 1107–1128.

5. Bru, D., Devaux, J., Bergheau, J. M., and Pont, D. 1997. Influence of material properties at high temperatures on the modelling of welding residual stress and deformation state. *Mathematical Modelling of Weld Phenomena* (3). Eds. H. Cerjak and H. K. D. H. Bhadeshia. The Institute of Materials, London, pp. 456–463.

6. Schwenk, C. 2007. FE-simulation of welding distortions of laser beam welded thin sheets — Sensitivity analysis through variation of the material properties. PhD dissertation, Berlin, Technische Universität.

7. Richter, F. 1973. The most important physical properties of 52 ferrous materials. *Stahleisen-Sonderberichte* (8). Verlag Stahleisen mbH, Düsseldorf.

8. Richter, F. 1983. Physical properties of steels and their temperature dependency — Polynomials and graphical display. *Stahleisen-Sonderberichte* (10). Verlag Stahleisen mbH, Düsseldorf.

9. Makhnenko, W. I. 1976. *Calculation Methods for the Investigation of the Kinetics of Welding Residual Stresses and Deformations*. Kiev.

10. N. N. 1990. Set-up of continuous cooling transformation diagrams for ferrous alloys. *Stahl-Eisen-Prüfblätter* (1680). Verlag Stahleisen GmbH, Düsseldorf.

11. Caron, J., Heinze, C., Schwenk, C., Babu, S. S., Lippold, J., and Rethmeier, M. 2010. Effect of continuous cooling transformation variations on numerical calculation of welding-induced residual stresses. *Welding Journal* 89(7): 151–160.

12. Thyssenkrupp Steel. 2002. *ThyssenKrupp Stahl Werkstoffblatt 1800: DP-W 550 and DP-W 600*.

13. Thyssenkrupp Steel 2000. *ThyssenKrupp Stahl Werkstoffblatt: NIROSTA H 400*.

14. Schuster, J. 1997. *Welding of Ferrous and Nickel-Base Alloys: Guideline for Practical Welding Metallurgy*. Fachbuchreihe Schweißtechnik, Volume 130, Düsseldorf, DVS-Verlag.

15. Alcan Rolled Products Europe/Alcan Automotive. 2002. *Technical Sheet Ecodal-608 (AA 6181A)*.

16. Merkel, M., and Thomas, K.-H. 2000. *Handbook of Materials*. Volume 5, Leipzig, Fachbuchverlag Leipzig.

17. DIN EN 573-3. 2003. *Aluminium and Aluminum Alloys: Chemical Composition and Geometry of Semifinished Products, Part 3: Chemical Composition*. Deutsches Institut für Normung e.V.

18. Zhang, Z., Sun, Q., Li, C., and Zhao, W. Theoretical calculation of the strain-hardening exponent and the strength coefficient of metallic materials. *Journal of Materials Engineering and Performance* 15(1): 19–22.

19. DIN SPEC 32534-1: *Numerical Welding Simulation — Execution and Documentation — Part 1: Overview*. Deutsches Institut für Normung DIN e.V., 2011.

Appendix A: Material Properties for Numerical Welding Simulation

The following figures show the thermophysical and thermomechanical material properties for the three alloys considered in this paper. The data is based on the experimental values and has been measured, checked, and validated as stated in the previous sections. The intended use of this data is the macroscopic temperature field and corresponding welding induced distortions and stresses, namely a welding structure simulation, where data for temperatures up to approximately 2000°C are sufficient. Before an application of the data, e.g., for a welding process simulation where the temperatures can be much higher, these values have to be adapted, cross checked, and validated again because otherwise, most simulation software extrapolates the last given gradient and assumes a linear behavior which is, especially when reaching the evaporation temperature, not the case anymore. A more detailed discussion of the presented material properties and their sensitivity, i.e. their influence on the simulation results, can be found in Ref. 4.

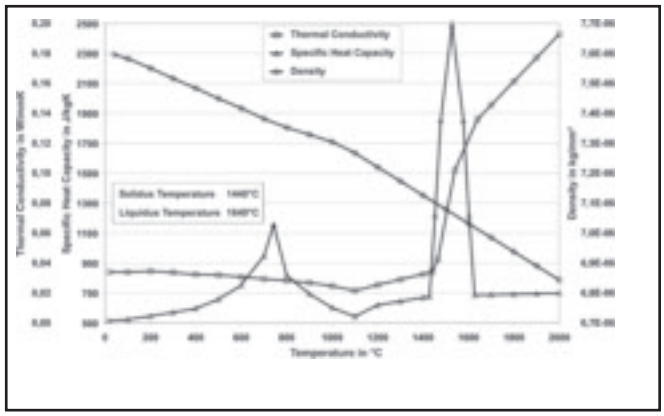

Fig. A1 — Temperature dependent thermophysical material properties of DP-W 600 (1.0936).

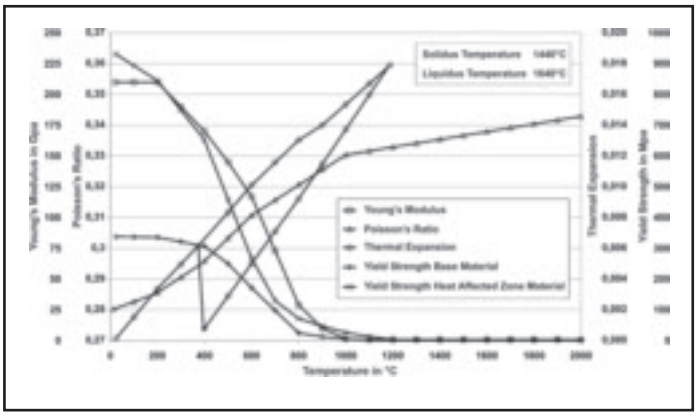

Fig. A2 — Temperature dependent thermomechanical material properties of DP-W 600 (1.0936).

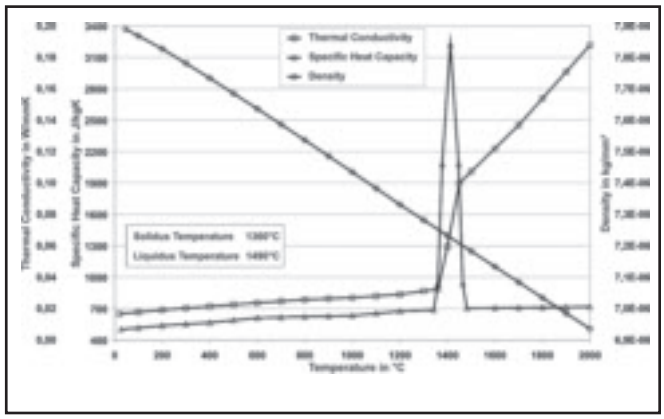

Fig. A3 — Temperature dependent thermophysical material properties of H400 (1.4376).

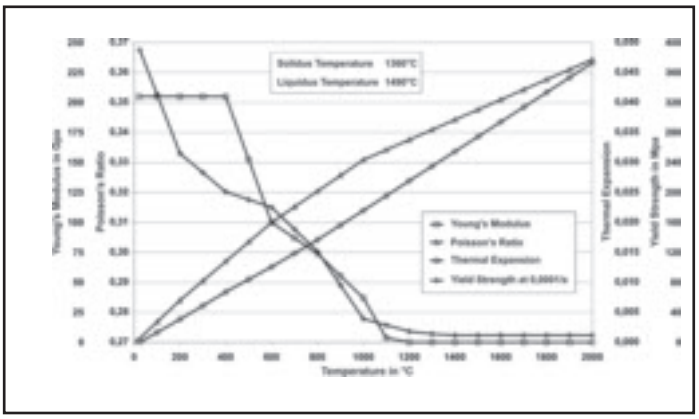

Fig. A4 — Temperature dependent thermomechanical material properties of H400 (1.4376).

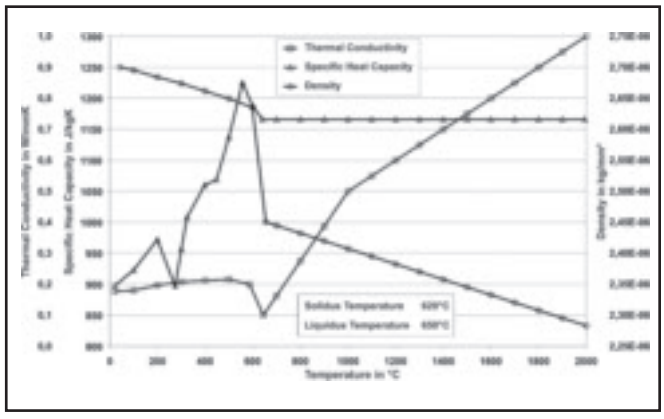

Fig. A5 — Temperature dependent thermophysical material properties of Ecodal 608 (EN AW-6181).

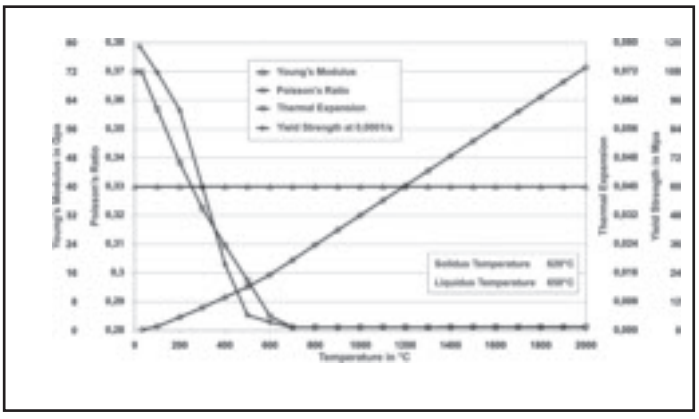

Fig. A6 — Temperature dependent thermomechanical material properties of Ecodal 608 (EN AW-6181).